Intermediate valence and non-Fermi liquid behavior in $Yb(Cu_ySi_{1-y})_{2-x}$, ($x=0.05-0.19$ and $y=0.12-0.15$)

V. H. Tran and D. Kaczorowski
W. Trzebiatowski Institute of Low Temperature and Structure Research, Polish Academy of Sciences, P.O. Box 1410, PL-50-950 Wrocław, Poland

A. Grytsiv and P. Rogl
Institut für Physikalische Chemie, Universität Wien, Währingerstr. 42, A-1090 Wien, Austria
(Received 4 April 2005; revised manuscript received 8 July 2005; published 22 September 2005)

We have investigated two ternary phases with close compositions: $Yb(Cu_{0.132}Si_{0.868})_{1.844}$ that crystallizes in the tetragonal $ThSi_2$-type structure with the lattice parameters $a=0.3981(1)$ and $c=1.3720(1)$ nm and $Yb(Cu_{0.145}Si_{0.855})_{1.883}$, which forms with a hexagonal structure of the AlB_2-type with $a=0.3926(1)$ and $c=0.3989(1)$ nm. Magnetic susceptibility, electrical resistivity, and specific heat measurements revealed considerably different magnetic behavior in the two ternaries. The $ThSi_2$-type compound is an intermediate valent material, characterized by a gap energy $E_{ex}=870$ K, a characteristic fluctuation temperature $T_{sf}=250$ K, and a coherence temperature $T_{coh}\sim 35$ K. In turn, the AlB_2-type phase is a Kondo lattice characterized by a Kondo temperature $T_K=58$ K. An enhanced electronic coefficient of the specific heat (~ 250 mJ/mol K^2 at 2 K) indicates strong renormalization of the quasiparticle masses in this material. Moreover, for the AlB_2-type compound we found several features characteristic of non-Fermi liquid systems: at low temperatures the magnetic susceptibility can be described by $\chi(T)\propto -T^{0.3}$, the electrical resistivity by $\rho(T)\propto T$, and the specific heat by $C/T\propto -T^{-1/2}$. The thermoelectric power and measurements confirm the difference in the magnetic behavior of these alloys.

DOI: 10.1103/PhysRevB.72.115116 PACS number(s): 71.10.Hf, 71.27.+a, 71.28.+d

I. INTRODUCTION

The study of strongly correlated electron systems (SCESs) is a very active field in modern condensed matter physics.[1] This fact is due to a variety of exotic phenomena discovered in SCESs, such as valence fluctuations, heavy-fermion behavior, non-Fermi liquid effect, and unconventional superconductivity. Despite many efforts many basic questions on the physics in SCESs still await answers, for instance, the mechanism of coexistence of superconductivity and heavy fermions or the nature of quantum critical behaviors. Among SCESs, cerium-based, ytterbium-based, and uranium-based compounds are frequently found to exhibit the exotic phenomena mentioned. This is because the *f*-electron shell in these three elements is unstable and in their compounds with *sp* elements and *d* elements it easily hybridizes with conduction electrons. As a result, the properties of such materials are governed by a competition between the Ruderman-Kittel-Kasuya-Yosida (RKKY) interaction with the characteristic temperature $T_{RKKY}\sim N(E_F)J^2$ and the Kondo effect characterized by an energy scale $T_K\sim\exp[-1/JN(E_F)]$.[2,3] These two basic interactions are related to the exchange constant J and the density of states at the Fermi level $N(E_F)$. As an important aspect, tuning J and/or $N(E_F)$, i.e., in consequence changing T_K and T_{RKKY}, one is able to push the system from one defined ground state to a different one. Experimentally, one can change J, e.g., by applying external pressure or, equivalently, by substitution of a suitable dopant (chemical pressure).

In the course of our systematic investigation of Yb-based intermetallic compounds,[4] we have recently found that a small quantity of Cu stabilizes a ternary phase with stoichiometry $Yb(Cu_ySi_{1-y})_{2-x}$, $x=0.05$–0.19 and $y=0.12$–0.15. Depending on exact composition, the material adopts two different crystal structure types: the tetragonal $ThSi_2$ type or the hexagonal AlB_2 type. In this paper we report on magnetization, electrical resistivity, and specific heat measurements performed on polycrystalline samples of both these phases. We show that by changing the composition one also varies the magnetic properties. While the sample with the $ThSi_2$-type unit cell (hereafter referred as sample 1) is a novel intermediate valence compound, the AlB_2-type compound (sample 2) exhibits local magnetism at high temperatures and a non-Fermi liquidlike behavior at low temperatures.

II. EXPERIMENTAL DETAILS

Polycrystalline samples with the nominal composition $Yb(Cu_{0.125}Si_{0.875})_2$ were synthesized by arc melting the constituent elements Yb (99.9 mass %), Cu (99.99 mass %) and Si (99.999 mass %) in a titanium-gettered argon atmosphere. Weight losses during the melting due to Yb evaporation were compensated beforehand to be less than 1% of the total mass in the final product. Two pieces from each sample were then vacuum sealed in quartz tubes and annealed at 650°C and 800°C for 140 h prior to quenching in cold water. X-ray examination of polycrystalline materials was performed at room temperature in a Guinier-Huber x-ray camera with an Image Plate recording system (CuKα1) employing an inter-

nal standard of 99.9999 mass % pure Ge (a_{Ge} = 0.565 790 6 nm). For Rietveld refinements we employed the FULLPROF program.[5] Light optical microscopy (LOM) on selected samples, which were polished and etched by standard methods, scanning electron microscopy (SEM) and electron microprobe analyses (EMPAs) based on energy dispersive x-ray spectroscopy [Si (Li) detector] were used to examine equilibrium compositions. For quantitative EMPAs the samples were analyzed employing an accelerating voltage of 20 kV for a counting time of 100 sec. X-ray energy spectra (Yb-Lα, Cu-Kα, and Si-Kα) were processed using the ZAF-4/FLS software package supplied by LINK SYSTEMS Ltd., England. Pure elements served as standards to carry out the deconvolution of overlapping peaks and background subtraction. Finally, the x-ray intensities were corrected for atomic number, absorption, and fluorescence effects using the TIMI program (Ref. 11). EMPA of the binary compound Yb_3Si_5 with narrow homogeneity region was used to evaluate an accuracy of the employed corrections and the obtained composition $Yb_{62.4}Si_{37.6}$ (at %) shows an excellent agreement with the real stoichiometry. Therefore, all compositions of the phases used in the article are after EPMA.

Magnetization M measurements were performed in the temperature range 1.7–800 K in magnetic fields up to 5 T using a Quantum Design Magnetic Property Measurement System (MPMS)-5 Super-conducting quantum interference device (SQUID) magnetometer. The electrical resistivity ρ was measured in the range 4.2–300 K employing a conventional dc four-point technique with a current of 10 mA. Specific heat, $C_p(T)$, measurements were performed in the temperature range 1.8–100 K, using an adiabatic method. The thermoelectric power S was measured between 4 and 300 K by a differential method.

III. RESULTS AND DISCUSSION

A. Composition range and crystal structure of $Yb(Cu_ySi_{1-y})_{2-x}$

EMPA of the samples shows almost a single-phase structure for an atomic content in the range of $Yb_{34.1-36.6}Cu_{7.6-10}Si_{55.3-56.8}$. Despite this narrow composition range, x-ray powder diffraction profiles unambiguously reveal the existence of two different structure types. The novel ternary compound coexisting in equilibrium with pure Si adopts $ThSi_2$-type structure, while the crystal structure of the ternary phase in the samples that are slightly enriched by Yb shows a close relation to the AlB_2 type. Based on these data the composition of both phases are expressed as $Yb(Cu_ySi_{1-y})_{2-x}$. Relation between both structure types is shown in Fig. 1.

Results of the Rietveld structural refinement of the $ThSi_2$-type structure are listed in Table I. A preliminary refinement, based on a simplified model assuming full occupancy of the 8c site [space group $I4_1/amd$, yields a good representation of the experimental diffraction intensities for composition $Yb_{33.9}Cu_{10}Si_{56.1}$ (at. %)]. For the composition $Yb_{35.2}Cu_{8.6}Si_{56.2}$, however, the structural refinement reveals Cu defects in the 8c site. Introducing EMPA data on the defect structure, the refinements with random occupation of

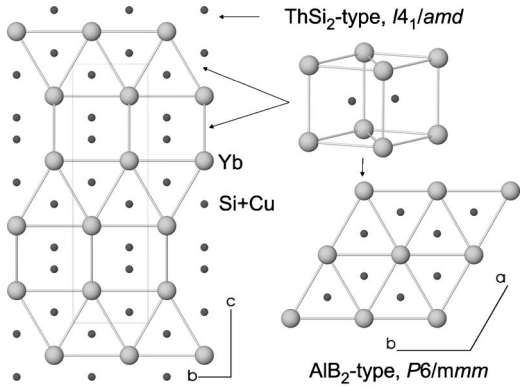

FIG. 1. Crystal structures of alloys $Yb(Cu_ySi_{1-y})_{2-x}$ with the $ThSi_2$ type and AlB_2 type.

Si and Cu atoms in the 8c sites show excellent agreement with observed data for both samples. Starting from the same nominal composition but arriving at a slightly higher Yb content in the as-cast alloy, sample 2 appears to be a single phase according to SEM and LOM. The x-ray powder diffraction pattern could be indexed with the AlB_2-type crystal structure yielding the lattice parameters a=0.39025(6) nm and c=0.3997(1) nm. Additional weak reflections could not be attributed to known ternary or binary phases from the Yb-Cu-Si system, which may indicate a supercell and/or a small quantity of secondary phases unidentified by SEM. On the other hand, as-cast samples with higher Yb content contain binary YbSi with CrB type; all peaks in the x-ray diffraction profile are attributed to this two-phase mixture of the ternary phase (AlB_2-structure type) and binary YbSi. In Table II we show the results of the Rietveld refinement. The crystallographic data were standardized using Program Structure Tidy.[6] Clearly, the data for the AlB_2-type phase may confirm the suggestion of vacancies in the Si sublattice (1a site) obtained from EPMA data. In this context, the existence of a deficiency in Si-site binary $YbSi_{2-x}$ shall be mentioned, the crystal structure of which was found to derive from the AlB_2-structure type.[4] The dependence of the lattice parameters of the AlB_2 phase on the Cu content is presented in Fig. 2 and compared with data on as-cast binary $YbSi_{2-x}$. One can see that, in agreement with the difference in atomic radii of Si and Cu atoms, the unit cell volume and a-lattice parameters increase, whereas c-lattice parameter and c/a ratio decrease. Finally, this tendency shows that interatomic distances between Yb atoms along [001] become almost equal to the Yb–Yb bond length in the $a-b$ plane. Notable is a decrease of the vacancy level (x) with Cu/Si substitution (y). Whereas the crystal lattice of the binary $YbSi_{2-x}$ with AlB_2-type structure has a significant defect ($0.26<x<0.33$),[4] a ternary phase with 9.5 at. % Cu contains only 17% of the vacancies in the 2b site. Around this Cu content appears a single-phase region of the ternary phase with $ThSi_2$ type. This compound shows a smaller level of the vacancies in the Si sublattice and much higher formula unit volume (see Fig. 2). The existence of two compounds with close composition offers a possibility to investigate the influence of crystal symmetry on physical properties. Therefore, two

TABLE I. Results of x-ray and electron microprobe analyses of $Yb(Cu_ySi_{1-y})_{2-x}$.

EMPA Data (at %)			$Yb(Cu_ySi_{1-y})_{2-x}$			Unit Cell Dimensions			
Yb	Cu	Si	x	y	Structure Type	a (nm)	c (nm)	V(nm^3)	Secondary Phases
35.21[a]	8.6	56.2	0.156	0.132	$ThSi_2$	0.3981(4)	1.3720(3)	0.2174(2)	eutectic with Si
34.1	9.3	56.6	0.067	0.141	$ThSi_2$	0.39857(4)	1.3777(3)	0.21886(6)	eutectic with Si
33.9	10.0	56.1	0.050	0.151	$ThSi_2$	0.39835(2)	1.3776(2)	0.21860(3)	eutectic with Si
35.62[a]	7.6	56.8	0.191	0.118	AlB_2	0.39025(6)	0.3997(1)	0.05271(2)	single phase
35.3	9.4	55.3	0.167	0.145	AlB_2	0.39261(1)	0.39893(2)	0.053251(4)	binary $Yb_{49.4}Si_{50.6}$

[a]Compositions used for measurements of the physical properties denoted as sample 1 and 2, respectively.

single-phase as-cast compositions $Yb_{35.2}Cu_{8.6}Si_{56.2}$ (tetragonal $ThSi_2$ type) and $Yb_{35.3}Cu_{9.4}Si_{55.3}$ (hexagonal AlB_2 type) were subjected to subsequent investigations.

B. Magnetic susceptibility and magnetization

The temperature dependence of the magnetic susceptibility of sample 1 is shown in Fig. 3. A broad maximum in the susceptibility is observed at around 140 K. This maximum is a characteristic feature of intermediate valent Ce-based and Yb-based compounds. There are several theoretical approaches to the intermediate valence (IV). In the so-called ionic-configuration-fluctuation (ICF) model[7] the rare-earth ion is assumed to fluctuate between the ground-state configuration and excited state configuration. In consequence, there are two relevant physical parameters: the energy difference between the two states E_{ex} and the effective fluctuation temperature T_{sf}, characterizing the width of the $4f$ band. For Yb-based compounds, the ground state could be the f^{14} con-

TABLE II. Structural data of $Yb(Cu_ySi_{1-y})_{2-x}$, standardized using Program Structure Tidy (Ref. 6).

Parameter	$Yb_{35.2}Cu_{8.6}Si_{56.2}$[a]	$Yb_{35.3}Cu_{9.4}Si_{55.3}$[a]
Formula from EPMA	$Yb(Cu_{0.132}Si_{0.868})_{1.844}$	$Yb(Cu_{0.145}Si_{0.855})_{1.883}$
Formula from refinement	$Yb(Cu_{0.135}Si_{0.865})_{1.844}$	$Yb(Cu_{0.151}Si_{0.849})_{1.883}$
Structure type, space group	$ThSi_2$, $I4_1/amd$	AlB_2, $P6/mmm$
a (nm), Guinier	0.398 14(5)	0.39261(1)
c (nm), Guinier	1.3720(4)	0.398 93(2)
Reflections measured	42	20
θ range	$20<2\theta<100$	$20<2\theta<100$
Number of variables	20	19
$R_F=\Sigma\lvert F_o-F_c\rvert/\Sigma F_o$	0.024	0.026
$R_I=\Sigma\lvert I_o-I_c\rvert/\Sigma I_o$	0.032	0.035
$R_{wP}=[\Sigma w_i\lvert y_{oi}-y_{ci}\rvert^2/\Sigma w_i\lvert y_{oi}\rvert^2]^{1/2}$	0.088	0.086
$R_P=\Sigma\lvert y_{oi}-y_{ci}\rvert/\Sigma\lvert y_{oi}\rvert$	0.068	0.111
$R_e=[(N-P+C)/\Sigma w_i y_{oi}^2)]^{1/2}$	0.022	0.019
$\chi^2=(R_{wP}/R_e)^2$	16.0	32.7
	atom parameters	
Yb	$4a(0,3/4,1/8)$	1a (0, 0, 0)
$B_{iso}(10^2$ nm$^2)$	1.29(1)	1.68(2)
Si+Cu	6.38(2)Si+0.99Cu	1.556(5)Si+0.277Cu
	$8e[0,1/4,0.2912(1)]$	$2d(1/3,2/3,1/2)$
$B_{iso}(10^2$nm$^2)$	1.71(3)	2.47(4)
	Interatomic distances [nm]	
	Yb-4Yb: 0.3966	Yb-6Yb: 0.3926
	Yb-4Yb: 0.3981	Yb-2Yb: 0.3989
	Yb-4Si: 0.3036	Yb-12Si: 0.3019
	Yb-8Si: 0.3036	
	Si-Si: 0.2275	Si-3Si: 0.2667
	Si-2Si: 0.2302	

[a]Compositions from EPMA.

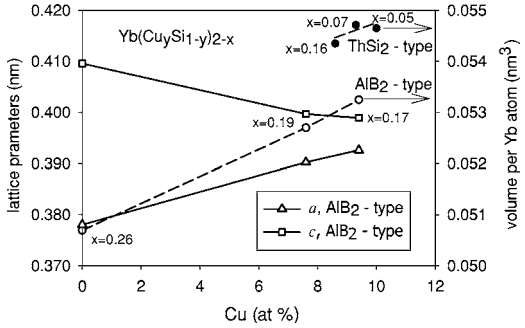

FIG. 2. Lattice parameters and unit cell volumes of $Yb(Cu_ySi_{1-y})_{2-x}$ as a function of Cu contents.

figuration with the total momentum $J=0$ and the effective magnetic moment $\mu_{eff}=0$, while the excited state could correspond to Yb^{3+} with the f^{13} configuration, for which $J=7/2$ and $\mu_{eff}=4.54\mu_B$. Accordingly, the susceptibility of Yb-based intermediate valent compounds may be accounted for using the formula[7]

$$\chi(T)=\frac{N_A 4.54^2 \mu_B^2[1-\nu(T)]}{3k_B(T+T_{sf})}+\chi_0 \qquad (1)$$

where the fractional occupation of Yb^{3+} states is given as $\nu(T)=1/[1+8\exp(-E_{ex}/k_B(T+T_{sf}))]$. The term χ_0 is the temperature independent susceptibility accounting for conduction electrons contribution (Pauli paramagnetism). The measured susceptibility of IV compounds often shows a rise at low temperatures, in most cases owing to some spurious magnetic contribution of Yb^{3+} ions. For sample 1, an upturn in the susceptibility is observed below 60 K. As will be shown below, it is probably due to a small quantity of antiferromagnetic impurity Yb_2O_3 with the Néel temperature of 2.3 K.[8] Therefore, in order to analyze the susceptibility of sample 1, we have taken into account the principal contribution from the fluctuating valence, as given in Eq. (1), and additionally a term describing the contribution of impurities. Assuming the Curie-Weiss behavior of the susceptibility of impurities $\frac{C_{imp}}{T-\Theta_{imp}}$, we obtained the following fit parameters: $E_{ex}=872(10)$ K and $T_{sf}=250(5)$ K, $C_{imp}=0.05(1)$ cm^3 K/mol, $\Theta_{imp}=-7(2)$ K, and $\chi_0=3.57(0.5)\times10^{-3}$ cm^3/mol. From the value of C_{imp} the amount of stable Yb^{3+} ions in the sample was estimated to be 1.3 at. %. The valence of intrinsic Yb ions in the sample can be deduced from the values of E_{ex} and T_{sf} to vary from 2.19 at 2 K up to 2.78 at 800 K. It should be noted that this valence change is comparable to those reported for other Yb-based intermediate valent compounds.[7,9] From Eq. (1), one may calculate the susceptibility at 0 K, $\chi(0)=3.59\times10^{-3}$ cm^3/mol.

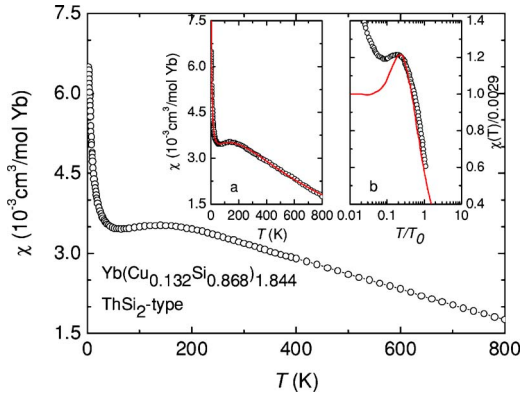

FIG. 3. (Color online) Temperature dependence of the magnetic susceptibility of sample $Yb(Cu_{0.132}Si_{0.868})_{1.844}$ measured at a field of 0.5 T. In the insets we compare the experimental data to theoretical curves. The solid line in the inset (a) is the fit using the ICF model, while in the inset (b), the solid line is a simulated susceptibility based on calculations of Rajan for $J=7/2$, $T_0=750$ K.

Alternatively, the appearance of a broad maximum in the susceptibility of IV compounds can be explained in the framework of the Anderson impurity (AI) and/or Anderson lattice (AL) models,[10,11,13,14] which predict also the occurrence of a maximum in the specific heat. The mentioned models have recently been applied for a number of IV materials such as $YbXCu_4$,[15] $YbAl_3$,[16] and $CeNiSi_2$.[17] In principle, the thermodynamic properties of IV compounds can be scaled by the Kondo temperature T_K. Following the calculations within the Bethe ansatz of the Coqlin-Schrieffer model given by Rajan,[18] one can estimate T_K from the relation

$$T_0=\frac{N(N^2-1)\mu_B^2 g^2}{24\pi k_B \chi(0)} \qquad (2)$$

Applying $\chi(0)=3.59\times10^{-3}$ cm^3/mol, as derived above for sample 1, the orbital degeneracy $N=2J+1=8$ and $g=8/7$, one obtains $T_0=914$ K. Consequently, the Kondo temperature T_K amounts to $T_K=0.529T_0=483$ K.[18,19] Alternatively, one can estimate T_K from the position of the susceptibility maximum as shown in the inset (b) of Fig. 3. Comparing the experimental data with a simulated curve based on the calculations of Rajan, we obtained $T_K=395$ K and $\chi(0)=2.9\times10^{-3}$ cm^3/mol, which are somewhat smaller than the values derived above.

As far as the susceptibility of sample 2 is considered, the Curie-Weiss (CW) law is obeyed for the experimental data over a wide temperature range 50–400 K. This fact implies a localized electron magnetism of the Yb ions in this compound. From the fit of the experimental data to the CW law (inset of Fig. 4), the paramagnetic Curie temperature of −140 K and the effective magnetic moment of $4.1\mu_B$ were deduced. The negative Θ_p value strongly suggests that in this sample the antiferromagnetic interactions dominate. The observed μ_{eff} value is comparable to the value of the free Yb^{3+} ions. Below 50 K, the susceptibility deviates from the Curie-Weiss law, suggesting an influence of crystalline electric field (CEF) effect and/or some magnetic correlations between the Yb ions.

In Fig. 5 we compare the susceptibility and magnetization data at low temperatures of the two investigated samples. Apparently, the susceptibility of sample 2 [panel (a)] is much larger than that of sample 1. At 1.8 K, χ of sample 2 reaches a value as large as 29.7×10^{-3} cm^3/mol, compared to about 6×10^{-3} cm^3/mol found in sample 1. In the case of the absence of any magnetic order, an enhancement in the suscep-

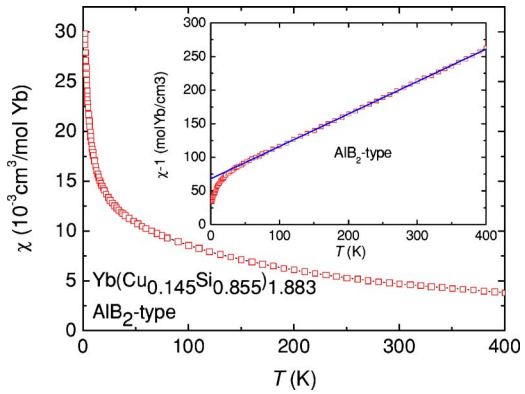

FIG. 4. (Color online) Temperature dependence of the susceptibility of sample 2 measured in a field of 0.5 T. The inset shows the Curie-Weiss law behavior of the sample.

tibility may imply a smaller value of the Kondo temperature. Using Eq. (2) and the measured value of the susceptibility of sample 2, one obtains T_K=58 K. A very interesting feature of the susceptibility of sample 2 is that below 5 K it scales with a power law, as illustrated by the solid line in Fig. 5(a). Fitting of the susceptibility data in the temperature range 1.7–5 K to the function $\chi(T)=\chi(0)-B*T^{\eta}$ yields η=0.3. The effect of electron correlations in sample 2 may be further assessed by examining the magnetic response on an applied magnetic field [Fig. 5(b)]. The magnetization data exhibit a clear curvature as a function of magnetic field and at the highest magnetic field applied (5 T) the magnetization is rather small ($0.21\mu_B$), compared to the value of $4\mu_B$ expected for free Yb^{3+} ions. The reduction in the magnetization value is probably caused by a combined effect of Kondo and CEF interactions. In turn, the magnetization of sample 1 is almost linear with respect to the field at least up to 2 T. The magnetization at 5 T is about four times smaller than that of sample 2.

C. Specific heat

In Fig. 6 we show the specific heat data measured at 0 T and 5 T for sample 1, in the form of the ratio C_p/T versus T. The C_p/T ratio at 0 T shows an upturn below about 5 K,

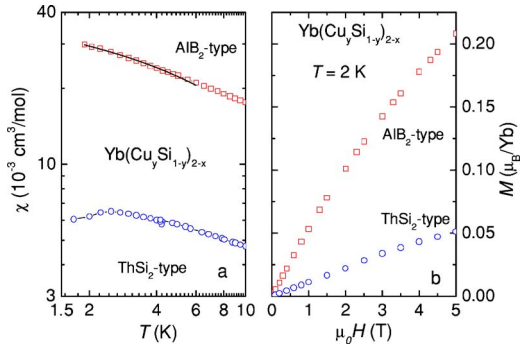

FIG. 5. (Color online) (a) Temperature dependence of susceptibility at low temperatures in the log-log scale. (b) Magnetization as a function of fields at 2 K.

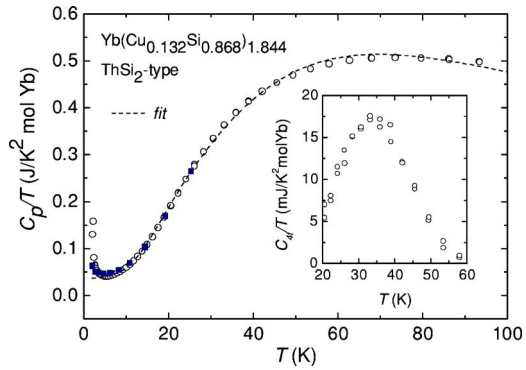

FIG. 6. (Color online) Temperature dependence of the specific heat divided by temperature of sample 1. The open points are data collected at the zero field, while solid squared points are collected at 5 T. The dashed line is the fit involved in the electric and phonon contributions to the specific heat. The inset shows the $4f$-electron contribution to the specific heat C_{4f}/T as a function of temperature.

reaching a value of about 150 mJ/K^2 mol at 2 K. However, this upturn is somewhat influenced by a small amount of Yb_2O_3 impurity. The presence of this phase is reflected by maximum at 2.2 K in the $C_p/T(T)$ curve. In the temperature range 8.5–16 K the specific heat follows the relation

$$C_p(T) = \gamma T + \beta T^3 \tag{3}$$

with the electronic coefficient of the specific heat γ =37 mJ/mol K^2 and the coefficient of the low-temperature Debye approximation for the phonon contribution β =0.36 mJ/mol K^4. The value of γ is comparable to the value of archetypal intermediate valent compound $CePd_3$ (35 mJ/mol K^2).[20] An enhanced γ value in IV compounds is due to the high density of states at the Fermi level resulting from a strong hybridization between $4f$ and conduction electrons. It should be noted that in a magnetic field of 5 T the peak structure at 2.2 K is no longer visible, and the value of γ evaluated from Eq. (3) for the temperature range 7–16 K increases up to 43 mJ/mol K^2. This observation is consistent with the expected behavior of IV compounds in magnetic fields being smaller than the Kondo field $B_K \sim k_B T_K/\mu_B$.[21] The value of T_K can be estimated from the electronic specific heat using the Bethe-ansatz formula for J=7/2

$$T_K = \frac{4.7215\pi^2 R}{24\gamma}. \tag{4}$$

Applying this equation for γ=37 mJ/mol K^2 we obtained a Kondo temperature of 436 K, which is of the same order of magnitude as that deduced from the magnetic susceptibility data.

The obtained β value yields an estimate for the Debye temperature Θ_D=253 K. Bearing in mind that Eq. (3) for the specific heat of metals is valid at temperatures below $\Theta/10$ only, one should examine the lattice contribution at higher temperatures by considering a sum of the Debye function and an Einstein mode. These two basic phonon contributions are distinguished by the respective characteristic temperatures Θ_D and Θ_E as well as by the numbers of involved oscillators n_D and n_E

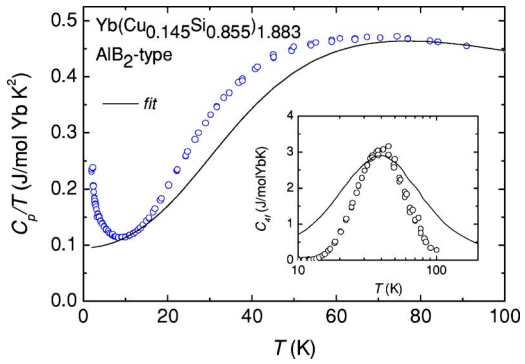

FIG. 7. (Color online) Temperature dependence of the specific heat divided by temperature of sample 2. The dashed line is the theoretical curve, simulated from the values Θ_D=280 K, Θ_E =110 K, n_D=2, and n_E=1. The inset shows the difference between the experimental specific heat data and theoretical ones, which is assumed to be the contribution of 4*f* electrons.

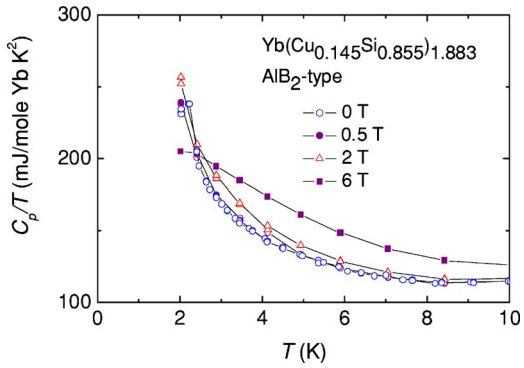

FIG. 8. (Color online) Temperature dependence of the specific heat divided by temperature of sample 2 measured at several magnetic fields.

$$C_{latt} = 9n_D k_B \left(\frac{T}{\Theta_D}\right)^3 \int_0^{\Theta/T} \frac{x^4 e^x}{(e^x - 1)^2} dx + 3n_E \frac{(\Theta_E/T)^2 e(\Theta_E/T)}{(e^{\Theta_E/T} - 1)^2}. \quad (5)$$

Fitting Eq. (5) to the experimental data of sample 1 between 5 K- and 100 K (taking into account the electronic contribution C_{el}) we obtained: Θ_D=280 K, Θ_E=98 K, n_D=2.1, and n_E=0.4. The result of the fit is shown in Fig. 6 by a dashed line. It is worth noting that the presence of the Einstein mode may be justified by plotting the C_p/T^3 data vs T. In fact this curve for sample 1 exhibits a clear maximum at about 20 K, which implies roughly Θ_E=100 K. An interesting finding is that the sum of n_D and n_E gives the total number of oscillators being smaller than three. This feature possibly reflects the presence in sample 1 of some defects in the crystallographic site occupancies. Another interesting observation comes out from the subtraction of the phonon contribution from the total C_p data. It is a broad maximum at around 34 K, which matches with a maximum near this temperature in the temperature derivative of electrical resistivity (see below). The existence of such maxima has been reported for some IV compounds that possess two energy scales[16,17] and ascribed to the coherence effect. Presumably a similar interpretation holds also for sample 1; however, one should take it with some caution until a suitable reference compound becomes available to provide a more reliable estimate of the 4*f* contribution to the measured specific heat.

In Fig. 7 we show the temperature dependence of the specific heat divided by temperature C_p/T for sample 2. C_p in the temperature range 9–15 K may be analyzed as a sum of two contributions as given in Eq. (3). From the fit, we obtained γ=95 mJ/mol Yb K^2 and β=0.267 mJ/mol K^4. The latter value corresponds to the Debye temperature of 280 K. Furthermore, we have plotted the C_p/T^3 data vs T to estimate the Einstein temperature and obtained a value of 110 K, similar to that determined for sample 1. The numbers of oscillators in sample 2 may be estimated from the C_p value at T=80 K, to be n_D=2 and n_E=1. Taking into account three different contributions, i.e., C_{el}, Debye, and Einstein modes, we have tried to fit the specific heat data for the whole temperature range. However, as is apparent from Fig. 7, no satisfactory conformity between the experimental and calculated data was obtained. Near 40 K the theory underestimates the magnitude of the specific heat by 3 J/mol Yb K. Since the theory reproduces the experimental data of sample 1 quite well, the origin of the problem encountered for sample 2 is unclear. Most likely it arises because of a substantial contribution of the 4*f* electrons, presumably originating from the Kondo and CEF effects. Ascribing the difference between the experimental specific heat and the calculated results to the 4*f*-electron contribution, we plotted the temperature dependence of C_{4f} in the inset of Fig. 7. One can see that the $C_{4f}(T)$ curve in the logarithmic temperature scale displays a Lorentzian shape, and this feature suggests that a Kondo-like mechanism is plausible. Hence, for comparison we show by the solid line the theoretical curve calculated within the Coqlin-Schrieffer model.[18] From this plot one may evaluate the Kondo temperature to be of 55 K, i.e., nearly the same as that deduced from the magnetic data.

Regarding the behavior of the specific heat at low temperatures, we see that the ratio C_p/T significantly rises below 10 K. Though there are some Yb_2O_3 impurities present that manifest themselves as a small anomaly at 2.2 K, we believe that the upturn in the C_p/T ratio below 8 K is intrinsic. In Fig. 8 we display the specific heat measured in several different magnetic fields. Apparently, in field lower than 2 T the C_p/T ratio measured at 2 K hardly changed with the increasing field and persists at the level of 250 mJ/mol K^2. In a field of 6 T the C_p/T ratio lowers to about 200 mJ/mol Yb K^2. Thus, the observed large specific heat contribution may be attributed to the effect of electronic correlations. Some more information about this feature may be obtained by examining the C_{4f}/T vs T plot (Fig. 9), where in the temperature range 3–8 K, one observes a power $T^{-1/2}$ law dependence. Clearly, a similar power law is not found in the specific heat of sample 1.

D. Electrical resistivity

The electrical resistivity of sample 1 as a function of temperature is displayed in Fig. 10. This curve clearly shows a metallic behavior. At low temperatures, $\rho(T)$ exhibits a

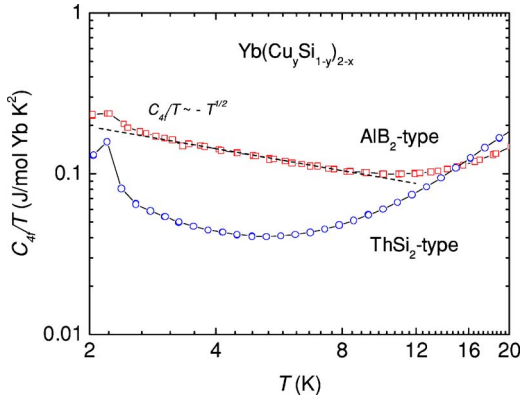

FIG. 9. (Color online) Temperature dependence of the magnetic specific heat divided by temperature. The dashed line presents a power $T^{-1/2}$ law. The solid lines are guides for the eye.

Fermi-liquid T^2 dependence with the prefactor A in the $\rho(T) \propto AT^2$ variation being equal to 0.012 $\mu\Omega$ cm. The ratio A/γ^2, known as the Kadowaki-Woods ratio,[22] amounts to 0.87×10^{-5} $\mu\Omega$ cm (mol K/mJ)^2, which is comparable to the common value of 1×10^{-5} $\mu\Omega$ cm (mol K/mJ)^2 for intermediate valence and heavy-fermion compounds.[22] The temperature derivative of the resistivity (see the inset of Fig. 10) shows a broad maximum near 37 K. We tentatively attribute this maximum to the coherence temperature in concord with the specific heat data. Besides, from the relationship between the ratio T_K/T_{coh} and the degeneracy $(2J+1)/\nu_f$,[11] one may expect that T_{coh} should be an order of magnitude smaller than T_K. For sample 1, assuming $T_K \sim 400$ K, one indeed gets $T_{coh} \sim 40$ K.

In Fig. 11 we show the temperature dependence of the electrical resistivity of sample 2. At the first glance, the resistivity behavior resembles those of dense Kondo compounds. A broad maximum in $\rho(T)$ is observed around 150 K and can be attributed to the overall crystalline electric field splitting, as already observed for YbNiSn.[12] A drop in the resistivity below the maximum may indicate that the coherence sets in. However, it should be noted that no Fermi-liquid-like behavior is seen below 10 K. Fitting the resistivity data in the temperature range 2–10 k to the power law form

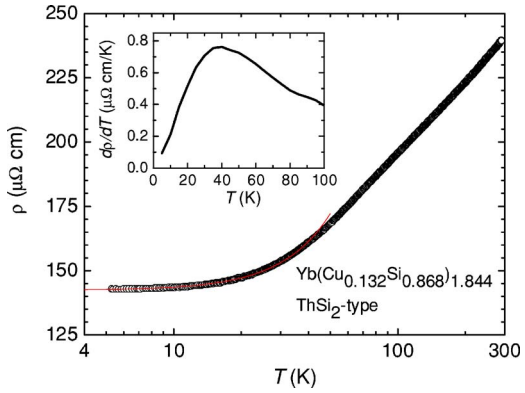

FIG. 10. (Color online) Temperature dependence of the electrical resistivity for sample 1. The solid line is a T^2 law. The inset shows the temperature derivative of the resistivity.

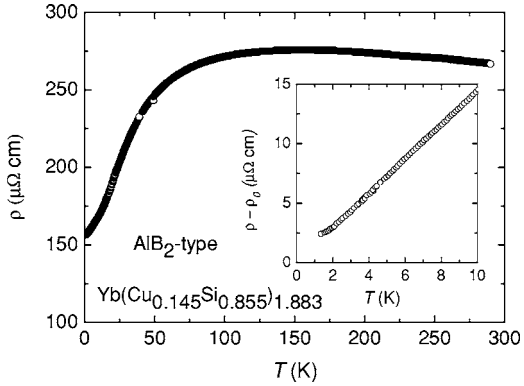

FIG. 11. Temperature dependence of the electrical resistivity for sample 2. The inset shows the low-temperature part of the resistivity.

$$\rho(T) = \rho_0 - AT^n, \tag{6}$$

we find that the exponent n appears to approach the constant value of 1 ± 0.1. Such a dependence of the resistivity points to a non-Fermi-liquid behavior of the compound. In this context we emphasize that both the magnetic susceptibility and the specific heat do exhibit non-Fermi-liquid dependencies, namely, $\chi \propto -T^{\eta}$ and $\gamma \propto T^{-1/2}$.

E. Thermoelectric power

The temperature dependencies of the thermoelectric power $S(T)$ for both studied samples of Yb(Cu$_{0.132}$Si$_{0.868}$)$_{1.844}$ and Yb(Cu$_{0.145}$Si$_{0.855}$)$_{1.883}$ are shown in Fig. 12. The Seebeck coefficient of sample 1 is negative in the whole temperature range measured. At room temperature, S amounts to -11 μV/K, which exceeds almost by one order of magnitude the values characteristic of simple metals like Cu and Au. The thermopower of sample 1 shows a broad minimum at $T_{min}=80$ K and a maximum at $T_{max}=140$ K. The former feature arises presumably due to Kondo scattering on the crystalline electric field ground state;[23] whereas the latter has no clear explanation yet, though interestingly T_{max} coincides with the position of the maximum in the magnetic susceptibility.

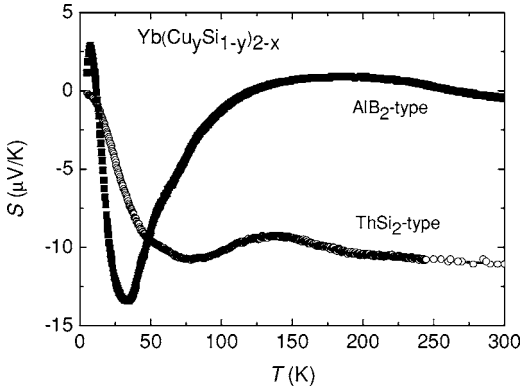

FIG. 12. Temperature dependence of the thermoelectric power of Yb(Cu$_{0.132}$Si$_{0.868}$)$_{1.844}$ and Yb(Cu$_{0.145}$Si$_{0.855}$)$_{1.883}$.

For intermediate valence systems, the $S(T)$ dependence at high temperatures is usually described by the formula[24]

$$T/S = \frac{B^2 + T^2}{A} \tag{7}$$

with $A=2(\epsilon_f-\epsilon_F)/e$ and $B^2=3[(\epsilon_f-\epsilon_F)^2+\Gamma^2]/3\pi^2k_B$ where ϵ_f is the energy position of f-electron level, ϵ_F is the Fermi energy, and Γ stands for the width of the Kondo resonance peak having the Lorentzian shape. Fitting the $S(T)$ data in the temperature range 145–300 K, one can estimate the distance of the $4f$ level from the Fermi level, $\epsilon_f-\epsilon_F$, to be 11 meV, and the width of the Kondo peak $\Gamma=41$ meV. These values are comparable to those reported for other intermediate valent ytterbium compounds, e.g., $YbCu_2Si_2$ (8.2 and 20 meV, respectively)[25] and $Yb_2Pt_3Sn_5$ (5.6 and 30 meV, respectively).[26]

The temperature dependence of the thermopower of sample 2 is definitively different from that of sample 1. Within a large temperature range 100–300 K, the Seebeck coefficient is nearly zero, and only at low temperatures are some interesting features found. The S curve exhibits a deep minimum at approximately 30 K, at which the thermopower attains a noticeable value of -13 μV/K. Moreover, we recognize a pronounced maximum in the $S(T)$ curve around 7 K. The latter feature might possibly be associated with the onset of magnetic correlations, which lead to the non-Fermi-liquid (NFL) like behavior, as manifested in the $\chi(T)$, $C_{4f}(T)$, and $\rho(T)$ characteristics.

IV. CONCLUDING REMARKS

We have shown that $Yb(Cu_ySi_{1-y})_{2-x}$, $x=0.05$–0.19 and $y=0.12$–0.15 crystallizes in either tetragonal $ThSi_2$-type or hexagonal AlB_2-type structure. The results of magnetic susceptibility, specific heat, electrical resistivity, and thermoelectric power measurements indicated a distinct difference in the electronic properties between these samples. The tetragonal compound is a mixed-valent system, while the hexagonal one shows at low temperatures several features characteristic of a class of NFL systems: a linear dependence of the electrical resistivity, and power law divergences in the temperature dependencies of the magnetic susceptibility and the electronic specific-heat coefficient. The differences in the electronic properties between $Yb(Cu_{0.132}Si_{0.868})_{1.844}$ and $Yb(Cu_{0.145}Si_{0.855})_{1.883}$ samples seem consistent with a description in which the nature of the ground state depends on a sensitive balance between competing Kondo and RKKY interactions. The change in the composition brings about some modification of the density of state near the Fermi energy, which is accompanied with the change in the crystal structure. It appears that $N(E_F)$ of sample 1 is much lower than that of sample 2. In consequence, the Kondo temperature of sample 1 is higher, giving rise to intermediate valence behavior. To support this approach we may compare the unit cell volumes and the magnetic behavior of the mutually related AlB_2-type compounds, i.e., $YbSi_{2-x}$ ($V=50.82$ Å^3) is an intermediate valent,[27] while $Yb(Cu_{0.145}Si_{0.855})_{1.883}$ ($V=52.7$ Å^3) is a NFL system. The doping of some amounts of Cu clearly increases the unit-cell volume and thus increases distances between Yb and (Cu, Si) atoms. In other words, the exchange constant J becomes smaller owing to the Cu doping. This effect is equivalent to a weakening of the hybridization between the $4f$ and conduction electrons. In turn, the Kondo temperature decreases, allowing the system to pass into a non-Fermi-liquid state.

It is interesting that if one makes a comparison of the physical properties of sample 2 with those of other NFL materials, one would see, e.g., some similarities to solid solutions $U_{1-x}Y_xPd_2Al_3$ reported by Freeman *et al.*[28] These authors suggested the presence of the quantum critical point (QCP) near the composition $x=0.7$, as being the reason of the observation of the NFL behavior in these alloys. Furthermore, the studies of other NFL systems showing QCP, e.g., $CeCu_{6-x}Au_x$, $Ce_{1-x}La_xRu_2Si_2$,[29] and $YbRh_2(Si_{0.95}Ge_{0.05})_2$,[30] indicated that the antiferromagnetic instability is the key factor in their quantum criticality. In the case of $Yb(Cu_{0.145}Si_{0.855})_{1.883}$, a nearby magnetic instability seems evident from the fact that the magnetic behavior of this compound can easily be modified by slightly changing the concentration of the involved elements. However, the theory of quantum phase transitions[31] does not include crystallographic disorder effects, which are certainly important in the samples studied. In turn, a disorder-driven mechanism is the crucial ingredient of the model based on a distribution of Kondo temperatures[32] and of the Griffiths-phase model.[33,34] The latter approach considers both the presence of atomic disorder and the competition between RKKY and Kondo interactions, and hence seems to be more relevant for $Yb(Cu_{0.145}Si_{0.855})_{1.883}$. Yet, the comparison of the experimental data with the Griffiths-phase model shows that it properly accounts for the specific heat only, and no satisfactory description is provided for the susceptibility data. On the other hand, the magnetic studies of sample 2 were limited to the temperatures above 2 K; therefore, the Griffiths-phase model cannot be ruled out yet. For this reason, further experiments carried out at much lower temperatures and possibly also under hydrostatic pressure are highly desired to shed more light on the actual nature of the NFL-like behavior observed for this compound.

ACKNOWLEDGMENTS

The authors acknowledge support from the Austrian-Polish Scientific Exchange Program 19/2003. Two of us (V.H.T. and D.K.) also thank the Polish State Committee for Scientific Research for the support within Grant No. 4T08A-045-24.

[1] Proceedings of the International Conference on Strongly Correlated Electron Systems, SCES'2002, Krakow, Poland, July 2002 [Acta Phys. Pol. B **34** (2003)]; SCES'2004, Karlsruhe, July 2004, Physica **359-361** (2005).
[2] S. Doniach, in *Valence Instabilities and Related Narrow Band Phenomena*, edited by R. D. Parks (Plenum, New York, 1977), p. 169; Physica B & C **91**, 231 (1977).
[3] J. R. Iglesias, C. Lacroix, and B. Coqblin, Phys. Rev. B **56**, 11820 (1997); and references therein.
[4] A. Grytsiv, D. Kaczorowski, A. Leithe-Jasper, V. H. Tran, A. Pikul, P. Rogl, M. Potel, H. Noël, M. Bohn, and T. Velikanova, J. Solid State Chem. **163**, 178 (2002).
[5] J. Rodriguez-Carvajal, Physica B **192**, 55 (1993).
[6] E. Parthe, L. Gelato, B. Chabot, M. Penzo, K. Cenzual, and R. Gladyshevskii, *TYPIX Standardized Data and Crystal Chemical Characterization of Inorganic Structure Types* (Springer-Verlag, Berlin, 1994).
[7] B. C. Sales and D. K. Wohlleben, Phys. Rev. Lett. **35**, 1240 (1975).
[8] R. M. Moon, W. C. Koehler, H. R. Child, and L. J. Raubenheimer, Phys. Rev. **176**, 722 (1968).
[9] D. T. Adroja, S. K. Malik, B. D. Padalia, S. N. Bhatia, R. Walia, and R. Vijayaraghavan, Phys. Rev. B **42**, R2700 (1990).
[10] N. E. Bickers, D. L. Cox, and J. W. Wilkins, Phys. Rev. B **36**, 2036 (1987)
[11] A. J. Millis and P. A. Lee, Phys. Rev. B **35**, 3394 (1987).
[12] G. Sparn, J. D. Thompson, and A. Hamzić, J. Alloys Compd. **181**, 197 (1992).
[13] Y. Ono, T. Matsuura, and Y. Kuroda, J. Photogr. Sci. **60**, 3475 (1991).
[14] S. Burdin, A. Georges, and D. R. Grempel, Phys. Rev. Lett. **85**, 1048 (2000).
[15] J. M. Lawrence, P. S. Riseborough, C. H. Booth, J. L. Sarrao, J. D. Thompson, and R. Osborn, Phys. Rev. B **63**, 054427 (2001); and references therein.
[16] A. L. Cornelius, J. M. Lawrence, T. Ebihara, P. S. Riseborough, C. H. Booth, M. F. Hundley, P. G. Pagliuso, J. L. Sarrao, J. D. Thompson, M. H. Jung, A. H. Lacerda, and G. H. Kwei, Phys. Rev. Lett. **88**, 117201 (2002).
[17] E. D. Mun, Y. S. Kwon, and M. H. Jung, Phys. Rev. B **67**, 033103 (2003).
[18] V. T. Rajan, Phys. Rev. Lett. **51**, 308 (1983).
[19] A. C. Hewson and J. W. Rasul, J. Phys. C **16**, 6799 (1983).
[20] M. J. Besnus, J. P. Kappler, and A. Meyer, J. Phys. F: Met. Phys. **13**, 597 (1983).
[21] T. Graf, J. M. Lawrence, M. F. Hundley, J. D. Thompson, A. Lacerda, E. Haanappel, M. S. Torikachvili, Z. Fisk, and P. C. Canfield, Phys. Rev. B **51**, 15053 (1995).
[22] K. Kadowaki and S. B. Woods, Solid State Commun. **58**, 507 (1986).
[23] E. Bauer, Adv. Phys. **40**, 417 (1991).
[24] U. Gottwick, K. Gloos, S. Horn, F. Steglich, and N. Grewe, J. Magn. Magn. Mater. **47–48**, 536 (1985).
[25] K. Alami-Yadri and D. Jaccard, J. Low Temp. Phys. **114**, 135 (1999).
[26] Y. Muro, K. Yamane, M. S. Kim, T. Takabatake, C. Godart, and P. Rogl, J. Phys. Soc. Jpn. **72**, 1745 (2003).
[27] A. Iandelli, P. Palenzona, and G. L. Olcese, J. Less-Common Met. **64**, 213 (1979).
[28] E. J. Freeman, M. C. de Andrade, R. P. Dickey, N. R. Dilley, and M. B. Maple, Phys. Rev. B **58**, 16027 (1998).
[29] H. V. Löhneysen, *Encyclopedia of Materials: Science and Technology* (Elsevier Science Ltd., New York 2001), pp. 61–85.
[30] O. Trovarelli, J. Custers, P. Gegenwart, C. Geibel, P. Hinze, S. Mederle, G. Sparn, and F. Steglich, Physica B **312–313**, 401 (2002).
[31] A. J. Millis, Phys. Rev. B **48**, 7183 (1993); U. Zülicke and A. J. Millis, Phys. Rev. B **51**, 8996 (1995); L. B. Ioffe and A. J. Millis, Phys. Rev. B **51**, 16151 (1995).
[32] O. O. Bernal, D. E. MacLaughlin, H. G. Lukefahr, and B. Andraka, Phys. Rev. Lett. **75**, 2023 (1995).
[33] M. C. de Andrade, R. Chau, R. P. Dickey, N. R. Dilley, E. J. Freeman, D. A. Gajewski, M. B. Maple, R. Movshovich, A. H. CastroNeto, G. Castilla, and B. A. Jones, Phys. Rev. Lett. **81**, 5620 (1998).
[34] A. H. CastroNeto, G. Castilla, and B. A. Jones, Phys. Rev. Lett. **81**, 3531 (1998).